Doping Liquid Crystals of Colloidal Inorganic Nanotubes by Additive-Free Metal Nanoparticles

Cyrille Hamon, Emmanuel Beaudoin, Pascale Launois, Erwan Paineau

Doping Liquid Crystals of Colloidal Inorganic Nanotubes by Additive-Free Metal Nanoparticles

Cyrille Hamon,[*] Emmanuel Beaudoin, Pascale Launois and Erwan Paineau[*]

Université Paris-Saclay, CNRS, Laboratoire de Physique des Solides, 91405, Orsay, France

AUTHOR INFORMATION

Corresponding Author

*cyrille.hamon@universite-paris-saclay.fr *erwan-nicolas.paineau@universite-paris-saclay.fr

ABSTRACT. Doping liquid-crystal phases with nanoparticles is a fast-growing field with potential breakthroughs due to the combination of the properties brought by the two components. One of the main challenges remains the long-term stability of the hybrid system, requiring complex functionalization of the nanoparticles at the expense of their self-assembly properties. Here we demonstrate the successful synthesis of additive-free noble-metal nanoparticles at the surface of charged inorganic nanotubes. Transmission electron microscopy and UV-visible spectroscopy confirm the stabilization of metallic nanoparticles on nanotubes. Meanwhile, the spontaneous formation of liquid-crystals phases induced by the nanotubes is observed, even after surface modification with metallic nanoparticles. Small-angle X-ray scattering experiments reveal that the average interparticle distance in the resulting hybrids can be easily modulated by controlling electrostatic interactions. As a proof-of-concept, we demonstrate the effectiveness of our method for the preparation of homogeneous transparent hybrid films with a high degree of alignment.

TOC GRAPHIC

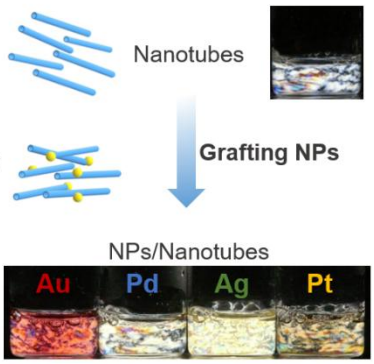

KEYWORDS. Imogolite, lyotropic mesophase, self-assembly, stability, SAXS, nanocomposite.

Inorganic lyotropic liquid-crystal (LC) are intermediate states of matter between ordered crystals and disordered liquids.[1] A wide variety of anisometric nanomaterials (e.g. rods, plates) self-organizes spontaneously in LC phases,[2–4] as a result of a gain in packing entropy ruled by excluded-volume interactions.[5] Research in this fast-growing field is motivated by the accurate control on the organization of individual particles, even at low volume fraction, over periodic distances up to the visible wavelength range and with significant response to external stimuli.[6–10]

In recent years, significant developments have been proposed by doping liquid crystal phases with inorganic nanoparticles (NPs), bringing new striking functionalities depending on the physical characteristic of these NPs.[11–13] For instance, noble metal NPs support light driven collective oscillations, known as surface plasmon resonances that can be merged with the characteristic properties of the LC host for applications such as chiral plasmonic metamaterials[14,15] or dynamic color displays.[16,17] Other NPs types such as quantum dots, iron oxides or ferroelectric metal oxides have been dispersed in LC host to form composite materials with enhanced electro-optical properties.[18,19] One of the main requirements in these composites is the long-term stability of NPs. To this end, NPs are frequently functionalized with an appropriate organic molecule to prevent aggregation and to facilitate their dispersion in the LC host.[20,21] Functionalized NPs have been conjugated at the surface of liquid-crystalline one-dimensional (1D) colloids. Typically, gold nanorods supported on carbon nanotubes as well as gold nanospheres supported on virus-rodlike particles have been obtained.[22,23] Although the supporting colloidal particles exhibit spontaneously liquid crystal phases without NPs,[24,25] self-assembly of the composite materials have not been shown. It presumably comes from the presence of surfactants or the relatively high ionic strength of the medium that may disturb liquid crystal phase in the hybrid materials.

Metal-oxide imogolite nanotubes (INTs) with chemical composition $(OH)_3Al_2O_3(Ge_{1-x}Si_x)(OH)$ offer many advantages as a host structure compared to other nanotubes.[26] Synthesized in aqueous media,[27–29] they readily form nematic and hexagonal columnar phases at low volume fractions (< 1%), which can be related to excluded-volume effects and the large intensity of repulsive interactions.[30,31] The high density of hydroxyl groups (~ 18 OH/nm²)[32] offers a high affinity for immobilization of metallic NPs on the outer surface.[33,34] In this sense, stable dispersion of nanoparticles immobilized on imogolite nanotubes have been obtained either by combination of preformed carboxylato-modified gold NPs[35] or by reducing metallic salts in situ in the host dispersion.[36–39] However, none of these studies reported the self-organization of the resulting hybrid system in LC phases. We hypothesize that methods limiting the uses of molecular additives would address this issue.

In this Letter, we built upon the seminal work of Liz-Marzán & Philipse[36,37] and on our experience in the LC phases of imogolite nanotubes[30,31] to study the self-organization of different NPs/INTs hybrids. Figure 1 illustrates the approach to prepare these hybrids. Details on the procedure are given in Supporting Information (SI). We synthesized first anisometric aluminogermanate double-walled INTs, in high yield by a wet chemical approach (**Figure 1**, step 1).[40] As-obtained dispersions were purified by dialysis and then concentrated by osmotic stress (**Figure 1**, step 2). Detailed characterization of the imogolite nanotubes are given elsewhere,[31,40] revealing monodisperse inner and outer diameters of 1.5 and 4.4 nm while the length distribution is relatively broad with an average length around 100 nm (**Figure S1**). Metallic salts (Au or Ag or Pd or Pt) were then reduced in situ using sodium borohydride without any surfactants or ligands (**Figure 1**, step 3). We fixed the final INT concentration at 8 $g.L^{-1}$, high enough to form an LC phase, and vary the metallic salt concentration during the synthesis (**Table S1**). The

dispersions were dialyzed against Milli-Q water to remove borate anions, prior further characterizations (**Figure 1**, step 4). The samples are named M_x hereafter, where M corresponds to the type of metal and the subscript *x* to the metal ratio (%w/v) in the hybrid sample.

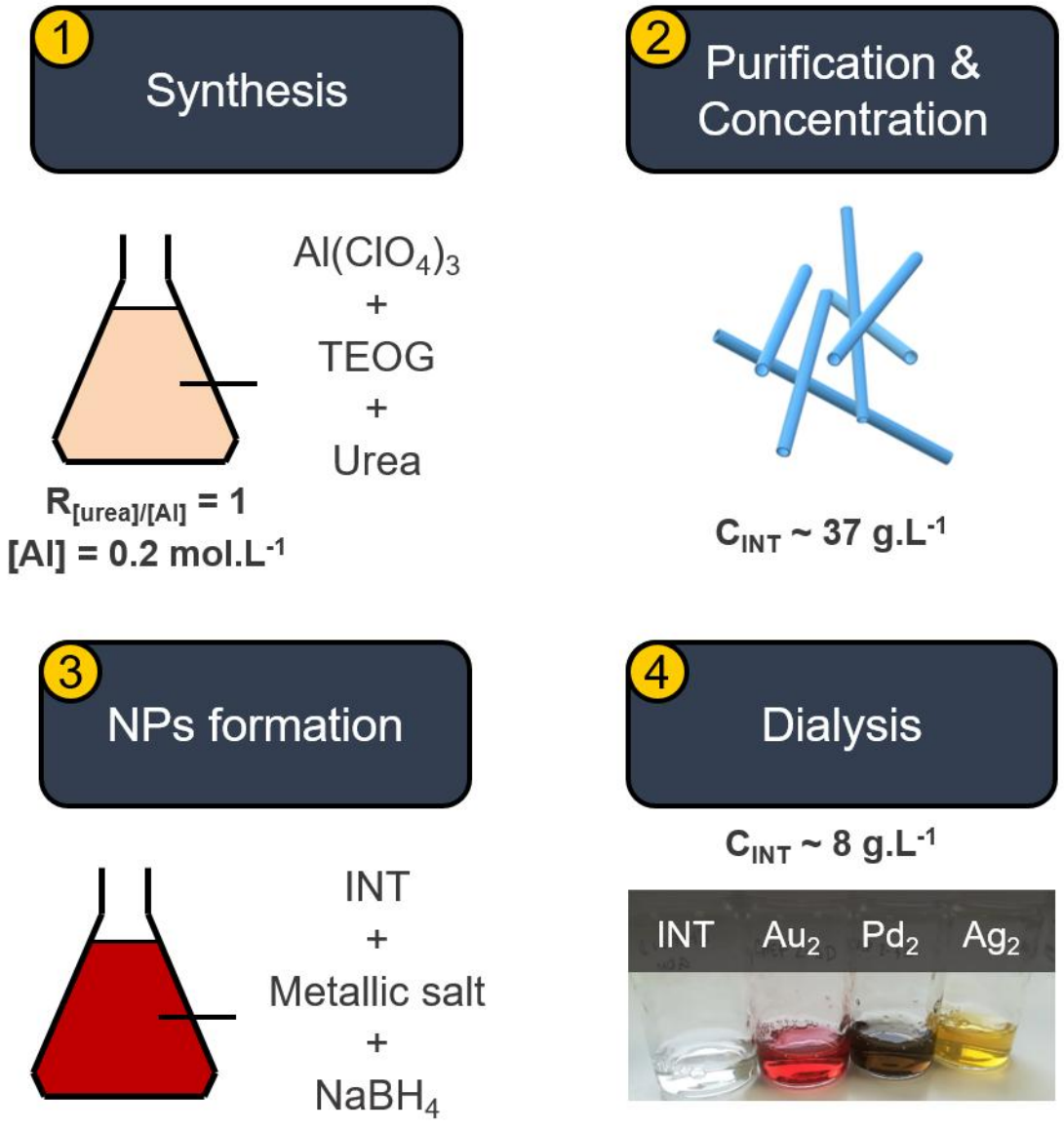

Figure 1. Schematic flowchart for the synthesis of NPs/INTs hybrids in aqueous media. TEOG corresponds to tetraethoxygermane.

The obtained NPs/INTs hybrids form colored dispersions that display birefringence when imaged between crossed polarizers (**Figure 2A**). This confirms the effective synthesis of stable

NPs in the liquid-crystalline host. The birefringent phases are limited however to the lowest concentration of metal (≤ 2% w/v). Samples prepared at higher metal ratio become isotropic (Pd_3, Pd_4) or exhibit either arrested phases (Ag_3, Ag_4, Pt_3 and Pt_4) or flocculation effects (Au_3, Au_4) (**Figure 2A and Figure S2**). These features could be induced by a change in the NP size, altering the electrostatic interactions between nanotubes. Indeed, the NPs should be smaller than the Debye screening length κ^{-1} ($\kappa^{-1} = 0.304/\sqrt{[IS]}$ with IS the ionic strength of the medium) to obtain stable colloidal dispersions.[36] After dialysis, the ionic strength of INTs suspensions is around 10^{-4} mol.L^{-1},[41] which corresponds to an electric double layer around nanotubes of 30 nm. Transmission Electron Microscopy (TEM) images confirmed the presence of small spherical NPs (3-6 nm) attached to the INTs with density as low as 1 NP/tube (**Figure S3**). Contrary to other 1D systems,[22,23] nanotubes are not decorated over their whole length and bare INTs are frequently observed. For metal ratio higher than 2% w/v, larger NPs size were observed with average size of 40-50 nm, i.e. more than ten times the outer INT diameter. In that case, NPs are no longer embedded inside the electric double layer of INTs, promoting the formation of flocs or arrested phase instead of LC phases (**Figure 2A**).

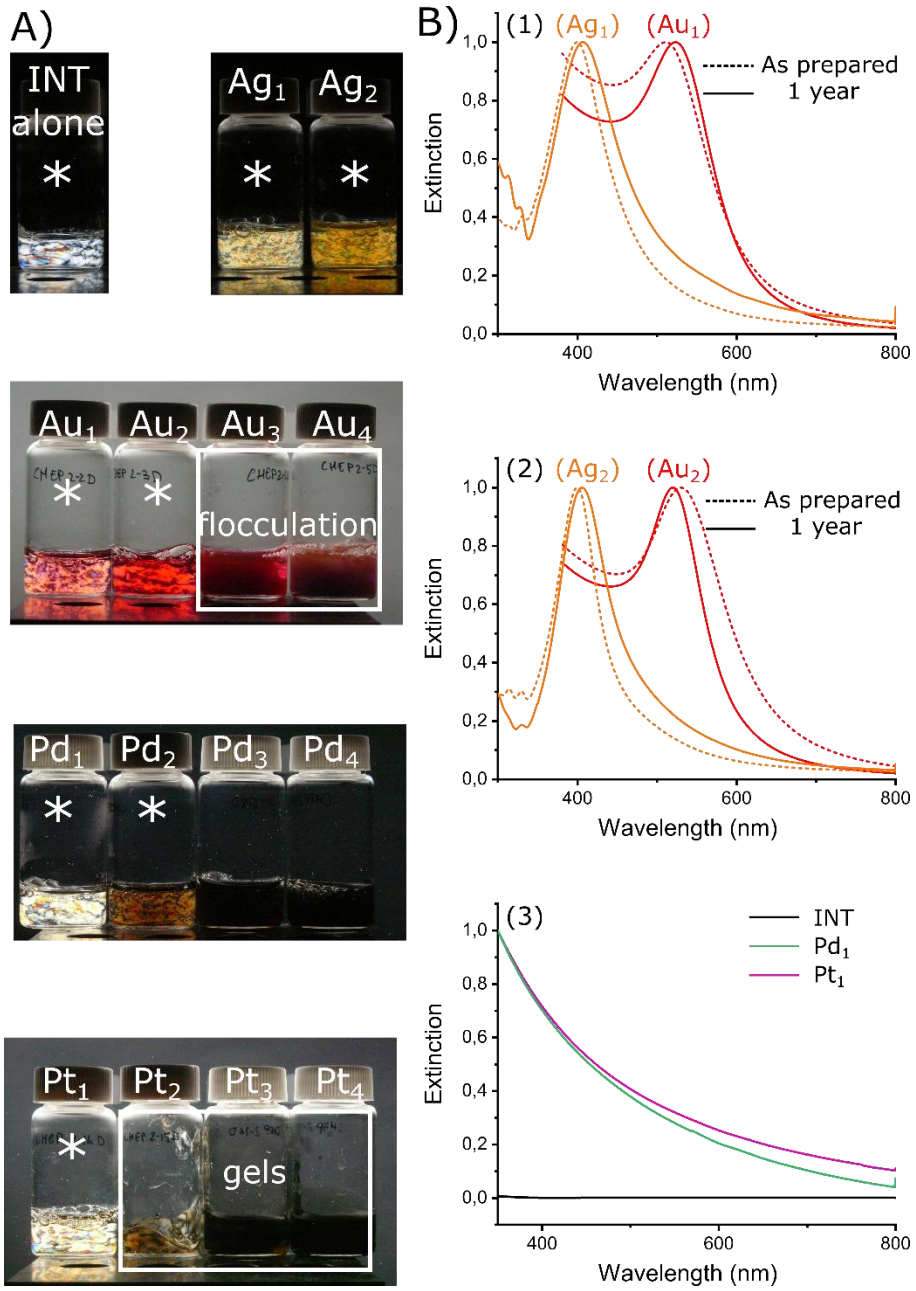

Figure 2. Colloidal dispersion after dialysis (IS < 10^{-4} M). A) Samples viewed in polarized light. Some samples are flocculated or turned as gels after dialysis, as noted on the images. Samples marked with an asterix (*) were used for further analysis in the following. B) Extinction spectra of the samples, just after synthesis (dashed lines) and 1 year after synthesis (solid lines). From top to bottom (1) Au_1 (red) and Ag_1 (orange), (2) Au_2 (red) and Ag_2 (orange), (3) pristine INTs (black), Pd_1 (green) and Pt_1 (magenta).

Au and Ag dispersions show ruby-red and yellow colors respectively, as expected for spherical NPs with plasmon resonance around 520 nm for Au and 400 nm for Ag (**Figure 2B**). For platinum and palladium hybrids, dispersions display a brown color with strong absorption below 500 nm in the UV-Vis spectra due to the scattering by the NPs. In all cases, our samples are found to be colloidally stable, as illustrated by the minor evolution of the plasmonic peaks over 1 year (**Figure 2B**).

Self-organization is investigated on the first two samples of each series, except for platinum nanoparticles that form gel samples for metal ratio higher than 1% w/v. Pure INTs sample is also prepared as a reference. For this purpose, batches of dispersions from each feedstock are equilibrated in dialysis membranes during two weeks with the appropriate amount of NaCl varying from 10^{-4} to 10^{-2} mol.L^{-1}. This allows the ionic strength to be fixed in the reservoir, avoiding any issues related to the Donnan effect.[42] Naked-eye and microscopic optical observations between crossed polarizers are presented in **Figure 3** and **Figure S4.**

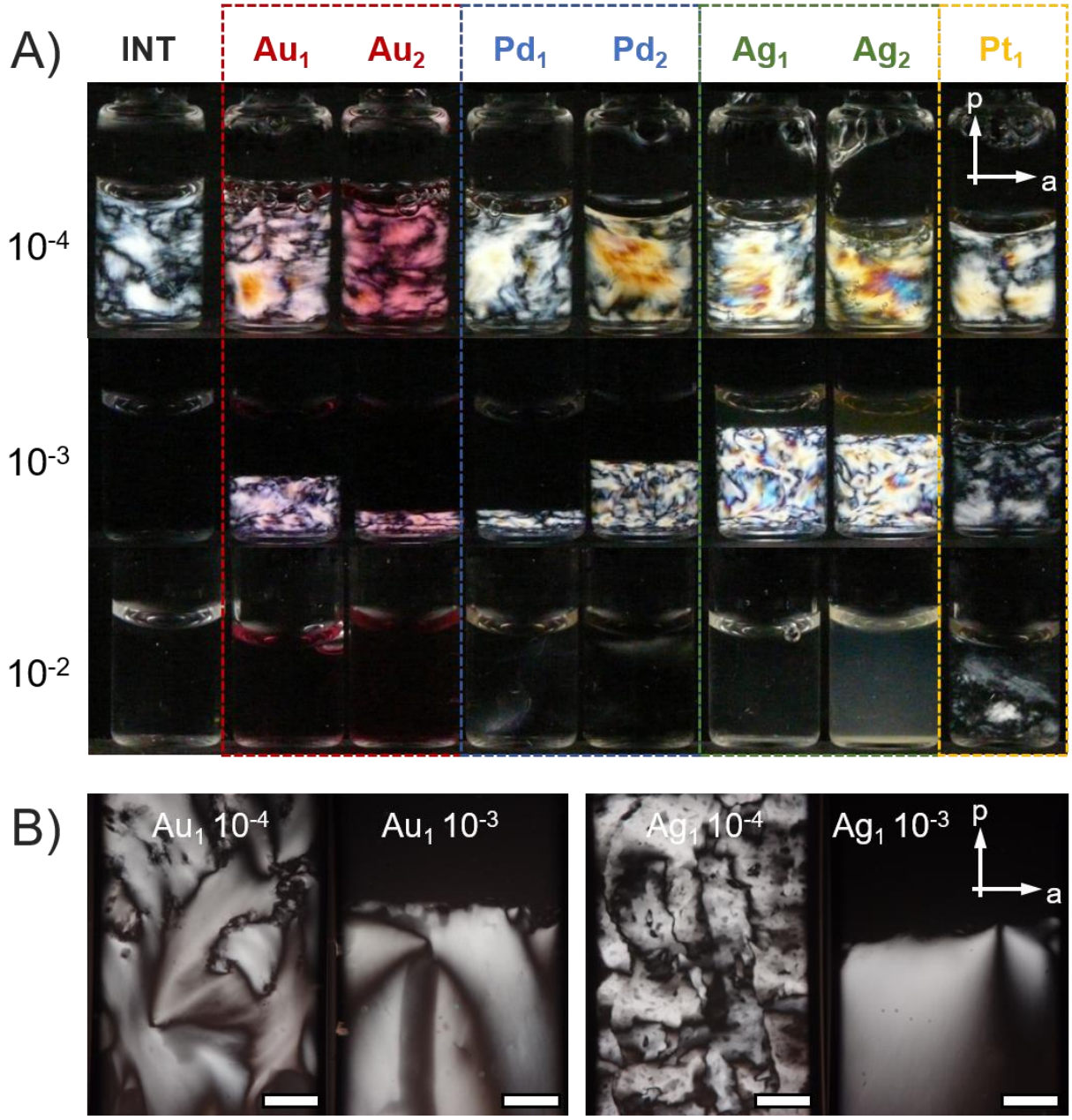

Figure 3. Effect of ionic strength on the self-assembly of NPs/INTs hybrids. A) Aqueous dispersions of NPs/INTs samples prepared at different ionic strength observed between crossed polarizer and analyzer. B) Textures in polarized optical microscopy for Au_1 (left) and Ag_1 (right) samples prepared at IS = 10^{-4} M and 10^{-3} M. The scale bar corresponds to 500 µm.

Although a detailed study of the phase diagram is out of scope of this study, some important conclusions can already be drawn. As mentioned before, aqueous dispersions of pure imogolite nanotubes may form spontaneously liquid-crystal phases at low volume fraction and ionic strength. Optical observations clearly evidence that the doping of INTs with additive-free noble-metal NPs do not suppress the occurrence of a liquid-crystal phase. Moreover, comparison with pure INT sample allows evidencing some modifications in the self-organization behavior. For IS = 10^{-4} mol.L^{-1}, all NPs/INTs hybrids form a fully birefringent fluid phase without phase separation as in INT reference sample (**Figure 3A**). Polarized optical microscopy (POM) reveals various optical textures depending on the metallic salt, which may originate from different kind of liquid-crystal phase.[30] For instance, Au_1 sample displays the typical 'Schlieren' texture of a nematic phase while that for Ag_1 is more complex (**Figure 3B**). The control of solvent ionic strength modulates the electrostatic interactions between charged nanotubes, allowing one to modify the self-organization behavior.[31,43] This is particularly true at IS = 10^{-3} mol.L^{-1} for which the Debye screening length remains large enough (κ^{-1} = 10 nm) to prevent attractive interactions. In this case, pure INT sample is isotropic since isotropic-to-columnar transition takes place at higher concentration than 8 g.L^{-1}.[31] In contrast, the stabilization of NPs allows a spontaneous phase separation resulting from the growth and coalescence of nematic tactoids (**Figure S4**). In addition, the amount of nematic phase appears to depend on both the nature of the metal and its ratio in the hybrid samples. Conversely, no liquid-crystalline phase is present at higher ionic strength and in the range of concentration investigated here (**Figure 3A**). These findings are corroborated by synchrotron-based small-angle X-ray scattering (SAXS) experiments. SAXS profiles for all NPs/INTs hybrids exhibit a Q^{-1} dependence of the scattered intensity, which is related to the form factor of one-dimensional objects (**Figure 4A-C**).

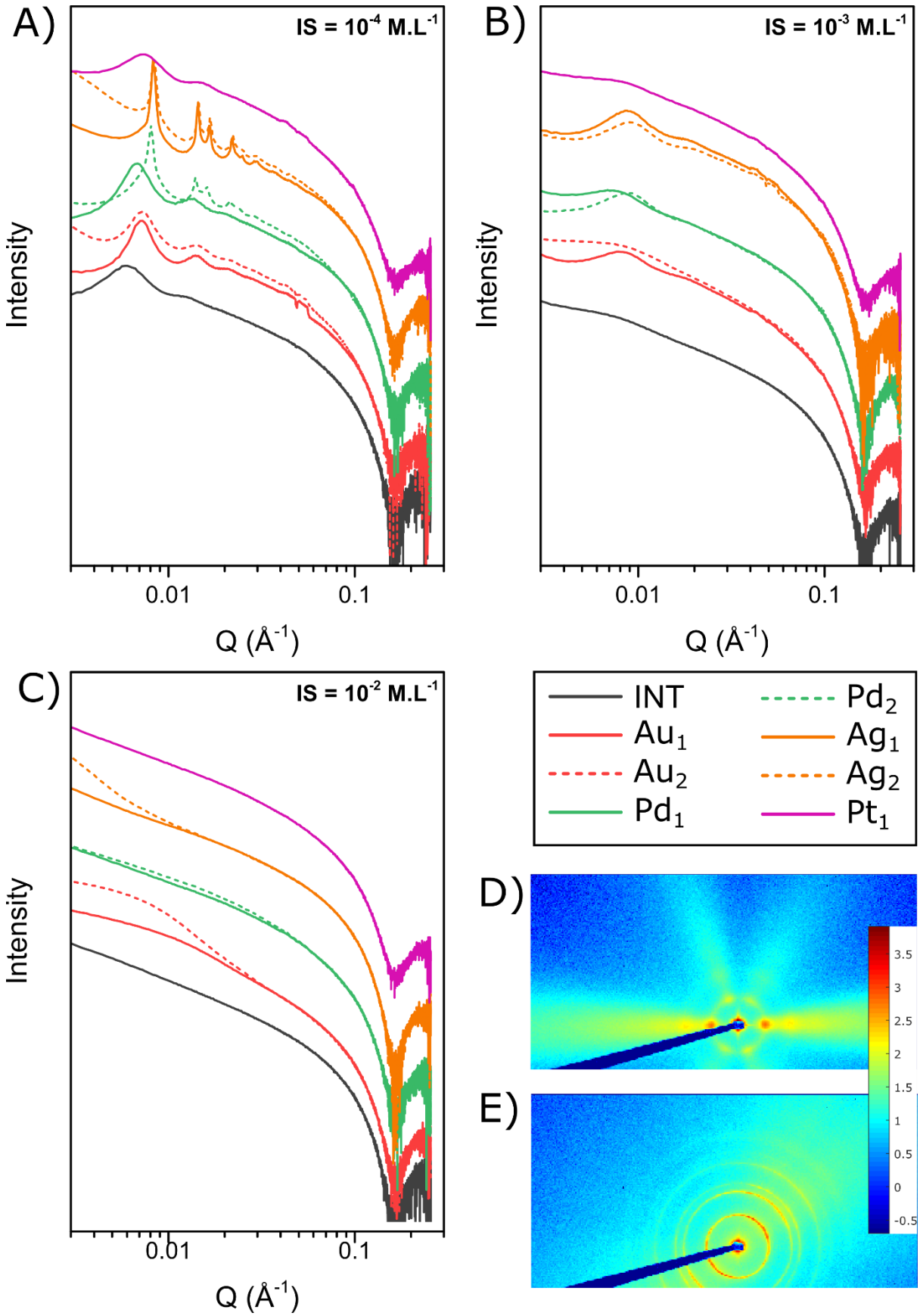
A)
IS = 10-4 M.L-1
Intensity
0.01
0.1
Q (Å-1)
B)
IS = 10-3 M.L-1
Intensity
0.01
0.1
Q (Å-1)
C)
IS = 10-2 M.L-1
Intensity
0.01
0.1
Q (Å-1)
INT
Au1
Au2
Pd1
Pd2
Ag1
Ag2
Pt1
D)
E)
3.5
3
2.5
2
1.5
1
0.5
0
-0.5

Figure 4. SAXS characterization of the suspension at different ionic strength. A-C) SAXS profiles of the suspensions at different ionic strength (A) 10^{-4} M.L^{-1}, (B) 10^{-3} M.L^{-1}, (C) 10^{-2} M.L^{-1}. (D-E) 2D SAXS images corresponding to the samples Au_1 and Ag_1 prepared at 10^{-4} M.L^{-1}, respectively.

SAXS patterns of birefringent samples are anisotropic, displaying several peaks related to the organization of the nanotubes in the LC phases (**Figure 4D-E**). For nematic samples, SAXS patterns display broad scattering peaks (**Figure 4A-B**) related to a liquid-like structure factor due to the short-range positional order of the nanotubes in the plane perpendicular to their long axis. The average correlation distance is estimated from the position of the maxima ($d = 2\pi/Q_{max}$). By contrast, Ag_1, Ag_2 and Pd_2 samples prepared at IS = 10^{-4} mol.L^{-1} display sharp Bragg reflections with Q-ratios of $1:\sqrt{3}:2:\sqrt{7}$ (**Figure 4A**), characteristic of a columnar phase with a long-range positional ordering of INTs on a hexagonal lattice perpendicular to the nanotube direction.[30,31] In that case, the average correlation distance corresponds to the lattice spacing of the columnar phase ($a = \sqrt{h^2 + k^2 + hk}\frac{4\pi}{Q_{hk}\sqrt{3}}$). In both cases, the correlation distances between the nanotubes slightly decrease when NPs are incorporated with a limited effect of the type of NPs and the metal ratio (**Table S2**). The lower values obtained for IS = 10^{-3} mol^{-1} point to a reduction in the extent of electrostatic interactions. The occurrence of only a nematic phase indicates that metal NPs inhibit long-range positional ordering of the nanotubes. Although the LC behavior is driven at the first order by INTs, the doping by additive-free NPs, even at low density, strongly modulates the self-organization of the resulting hybrid.

We demonstrate in the following that colloidal NPs/INTs hybrids can be easily processed as nanocomposite films with high degree of orientation. It is well known that INTs are readily dispersed in various polymer matrix.[44–46] Here, we use a water-soluble polymer, poly(vinyl

alcohol) (PVA), with a high molar mass (M_w = 195 000 g.mol^{-1}) in order to get a large degree of entanglements in the resulting nanocomposite films. After evaporation (see Supporting Information), free-standing films prepared from Au_1 sample and pure INTs, used here as a reference, appear uniform and transparent, which indicate the absence of aggregates (**Figure 5A-C**).

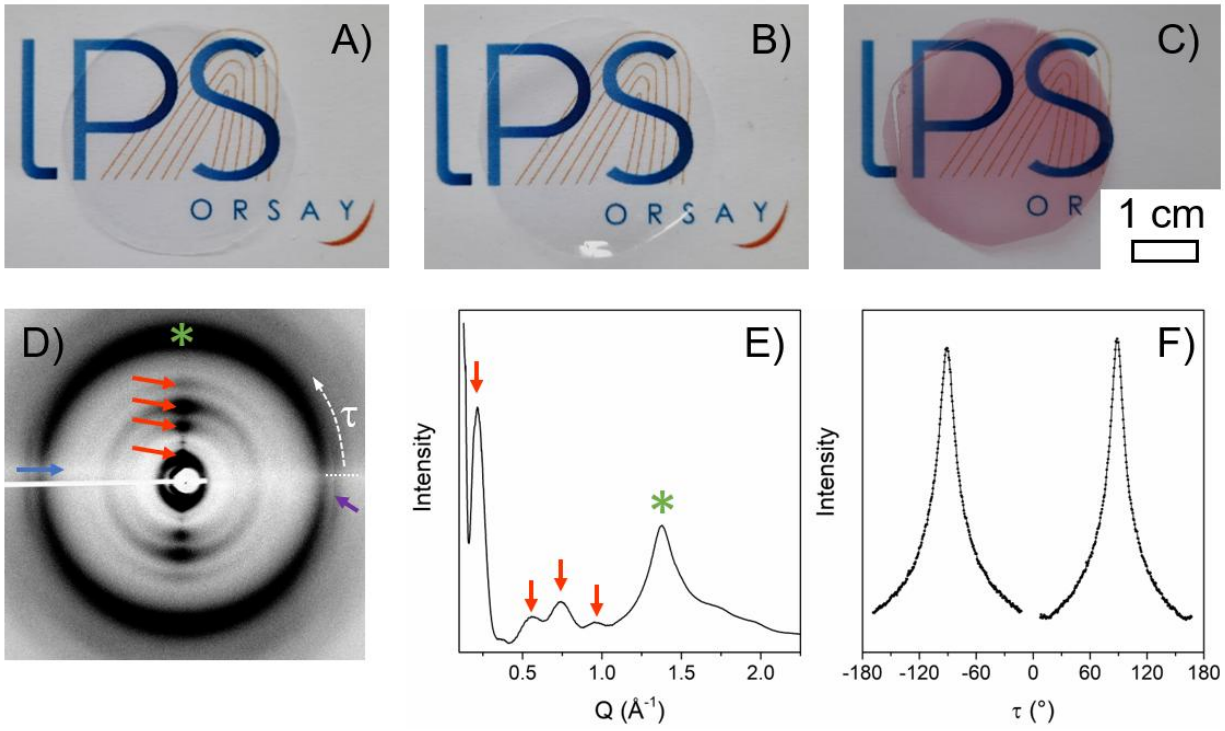

Figure 5. Images of (A) PVA, (B) PVA/INT and (C) PVA/Au_1 nanocomposite films. (D) WAXS pattern of PVA/Au_1 film oriented parallel to the X-ray beam. Horizontal blue arrow points the shadow of the film while red and purple arrows indicate the characteristic scattering features of the INTs. The green star corresponds to PVA scattering feature. (E) Integrated intensity as a function of the wave-vector and (F) intensity at Q = 0.22 Å^{-1} as a function of the angle τ on the scattering pattern.

PVA, PVA/INT and PVA/Au_1 have been studied by Wide-Angle X-ray scattering (WAXS). WAXS patterns are measured in two configurations, the film being either parallel or perpendicular to the X-ray beam. In perpendicular configuration, the scattering pattern is formed of isotropic rings. The PVA chains and imogolite nanotubes have random orientation in the plane of the film. Note that no signal from gold nanoparticles could be detected due to their small amount and size. The WAXS pattern of PVA/Au_1 film in parallel configuration is shown in **Figure 5D**. Quantitative textural analysis is beyond the scope of this article and it would be made difficult by the anisotropic absorption of the film in parallel configuration, leading to a shadow in WAXS patterns (**Figure 5D**). Nevertheless, we can draw some conclusions, which can also be apply to PVA and PVA/INT nanocomposite films. Red arrows in **Figure 5D-E** point towards oscillations characteristic of the squared form factor of double-walled nanotubes, located in their equatorial plane.[30,40] Their intensity are modulated angularly with maximum values at angles $\tau = 90$ and 270°, perpendicularly to the plane of the film, which shows that the nanotubes are preferentially oriented within this plane (**Figure 5D,E**). Conversely, the purple arrow refers to an intensity maximum, characteristic of the nanotubes periodicity along their long axis and it thus has maximum intensity at 0 and 180°. The modulation at Q ~ 1.4 $Å^{-1}$ corresponds to the distance between PVA chains.[47] Its intensity is maximum at $\tau = 90$ and 270°, which indicates that PVA chains are preferentially aligned within the nanotube film.

In summary, we demonstrate the feasibility to dope liquid-crystal phases of inorganic nanotubes by noble-metal nanoparticles without the use of molecular additives. Low concentration of metal (≤ 2% w/v) allows the formation of small spherical NPs stabilized by the nanotubes. The resulting hybrids are stable with time combining the self-organization behavior of nanotubes with the optical plasmon properties of noble-metal NPs. In particular, we evidence

that the LC order in these hybrid systems is strongly sensitive to the addition of NPs with size of the same order of magnitude as the nanotubes diameter. Potential application of NPs/INTs hybrids is illustrated for the preparation of transparent polymer nanocomposites films in which both nanotubes and polymer chains are preferentially oriented within the film plane. These results should certainly lead to further experimental findings with interests for optical devices and sensors or photoactive nanoreactors.

ASSOCIATED CONTENT

Supporting Information. The following files are available free of charge.

Experimental details including the synthesis of inorganic nanotubes, metallic nanoparticles/nanotubes hybrids and nanocomposite hybrid films, TEM observations and additional POM figures (PDF)

AUTHOR INFORMATION

Notes

The authors declare no competing financial interests.

ACKNOWLEDGMENT

The project has received financial support from Agence Nationale de la Recherche (grant number ANR-18-CE09-0001). TEM observations were performed at the Imagerie-Gif core facility supported by l'Agence Nationale de la Recherche (ANR-11-EQPX-0029/Morphoscope; ANR-10-INBS-04/FranceBioImaging; ANR-11-IDEX-0003-02/Saclay Plant Sciences). Authors gratefully acknowledge the SOLEIL synchrotron for awarding beamtime (20181790 and 20201118). The authors thank Doru Constantin for help during SAXS experiments and Stéphan Rouzière for the use of MORPHEUS platform.

REFERENCES

(1) De Gennes, P.-G.; Prost, J. *The Physics of Liquid Crystals*; Oxford university press, 1993; Vol. 83.

(2) Lekkerkerker, H. N. W.; Vroege, G. J. Liquid Crystal Phase Transitions in Suspensions of Mineral Colloids: New Life from Old Roots. *Philos. Trans. R. Soc. Math. Phys. Eng. Sci.* **2013**, *371*, 20120263.

(3) Liu, Y.; Xu, Z.; Gao, W.; Cheng, Z.; Gao, C. Graphene and Other 2D Colloids: Liquid Crystals and Macroscopic Fibers. *Adv. Mater.* **2017**, *29*, 1606794.

(4) Dierking, I.; Al-Zangana, S. Lyotropic Liquid Crystal Phases from Anisotropic Nanomaterials. *Nanomaterials* **2017**, *7*, 305.

(5) Onsager, L. The Effects of Shape on the Interaction of Colloidal Particles. *Ann. N. Y. Acad. Sci.* **1949**, *51*, 627–659.

(6) Michot, L. J.; Bihannic, I.; Maddi, S.; Funari, S. S.; Baravian, C.; Levitz, P.; Davidson, P. Liquid–crystalline Aqueous Clay Suspensions. *Proc. Natl. Acad. Sci.* **2006**, *103*, 16101–16104.

(7) Shen, T.-Z.; Hong, S.-H.; Song, J.-K. Electro-Optical Switching of Graphene Oxide Liquid Crystals with an Extremely Large Kerr Coefficient. *Nat. Mater.* **2014**, *13*, 394–399.

(8) Sano, K.; Kim, Y. S.; Ishida, Y.; Ebina, Y.; Sasaki, T.; Hikima, T.; Aida, T. Photonic Water Dynamically Responsive to External Stimuli. *Nat. Commun.* **2016**, *7*, 1–9.

(9) Frka- Petesic, B.; Radavidson, H.; Jean, B.; Heux, L. Dynamically Controlled Iridescence of Cholesteric Cellulose Nanocrystal Suspensions Using Electric Fields. *Adv. Mater.* **2017**, *29*, 1606208.

(10) Nakayama, M.; Kajiyama, S.; Kumamoto, A.; Nishimura, T.; Ikuhara, Y.; Yamato, M.; Kato, T. Stimuli-Responsive Hydroxyapatite Liquid Crystal with Macroscopically Controllable Ordering and Magneto-Optical Functions. *Nat. Commun.* **2018**, *9*, 1–9.

(11) Bisoyi, H. K.; Kumar, S. Liquid-Crystal Nanoscience: An Emerging Avenue of Soft Self-Assembly. *Chem. Soc. Rev.* **2011**, *40*, 306–319.

(12) Constantin, D.; Davidson, P. Lamellar Lα Mesophases Doped with Inorganic Nanoparticles. *ChemPhysChem* **2014**, *15*, 1270–1282.

(13) Dierking, I.; Martins Figueiredo Neto, A. Novel Trends in Lyotropic Liquid Crystals. *Crystals* **2020**, *10*, 604.

(14) Querejeta-Fernández, A.; Chauve, G.; Methot, M.; Bouchard, J.; Kumacheva, E. Chiral Plasmonic Films Formed by Gold Nanorods and Cellulose Nanocrystals. *J. Am. Chem. Soc.* **2014**, *136*, 4788–4793.

(15) Bagiński, M.; Tupikowska, M.; González- Rubio, G.; Wójcik, M.; Lewandowski, W. Shaping Liquid Crystals with Gold Nanoparticles: Helical Assemblies with Tunable and Hierarchical Structures Via Thin- Film Cooperative Interactions. *Adv. Mater.* **2020**, *32*, 1904581.

(16) Lesiak, P.; Bednarska, K.; Lewandowski, W.; Wójcik, M.; Polakiewicz, S.; Bagiński, M.; Osuch, T.; Markowski, K.; Orzechowski, K.; Makowski, M. Self-Organized, One-Dimensional Periodic Structures in a Gold Nanoparticle-Doped Nematic Liquid Crystal Composite. *ACS Nano* **2019**, *13*, 10154–10160.

(17) Neubrech, F.; Duan, X.; Liu, N. Dynamic Plasmonic Color Generation Enabled by Functional Materials. *Sci. Adv.* **2020**, *6*, eabc2709.

(18) Mirzaei, J.; Reznikov, M.; Hegmann, T. Quantum Dots as Liquid Crystal Dopants. *J. Mater. Chem.* **2012**, *22*, 22350–22365.
(19) Prakash, J.; Khan, S.; Chauhan, S.; Biradar, A. M. Metal Oxide-Nanoparticles and Liquid Crystal Composites: A Review of Recent Progress. *J. Mol. Liq.* **2020**, *297*, 112052.
(20) Stamatoiu, O.; Mirzaei, J.; Feng, X.; Hegmann, T. Nanoparticles in Liquid Crystals and Liquid Crystalline Nanoparticles. In *Liquid Crystals*; Topics in Current Chemistry; Springer, Berlin, Heidelberg, 2011; Vol. 318, pp 331–393.
(21) Liu, Q.; Yuan, Y.; Smalyukh, I. I. Electrically and Optically Tunable Plasmonic Guest–host Liquid Crystals with Long-Range Ordered Nanoparticles. *Nano Lett.* **2014**, *14*, 4071–4077.
(22) Dujardin, E.; Peet, C.; Stubbs, G.; Culver, J. N.; Mann, S. Organization of Metallic Nanoparticles Using Tobacco Mosaic Virus Templates. *Nano Lett.* **2003**, *3*, 413–417.
(23) Jiang, K.; Eitan, A.; Schadler, L. S.; Ajayan, P. M.; Siegel, R. W.; Grobert, N.; Mayne, M.; Reyes-Reyes, M.; Terrones, H.; Terrones, M. Selective Attachment of Gold Nanoparticles to Nitrogen-Doped Carbon Nanotubes. *Nano Lett.* **2003**, *3*, 275–277.
(24) Dogic, Z.; Fraden, S. Ordered Phases of Filamentous Viruses. *Curr. Opin. Colloid Interface Sci.* **2006**, *11*, 47–55.
(25) Davis, V. A.; Parra-Vasquez, A. N. G.; Green, M. J.; Rai, P. K.; Behabtu, N.; Prieto, V.; Booker, R. D.; Schmidt, J.; Kesselman, E.; Zhou, W. True Solutions of Single-Walled Carbon Nanotubes for Assembly into Macroscopic Materials. *Nat. Nanotechnol.* **2009**, *4*, 830.
(26) Paineau, E. Imogolite Nanotubes: A Flexible Nanoplatform with Multipurpose Applications. *Appl. Sci.* **2018**, *8*, 1921.
(27) Levard, C.; Rose, J.; Masion, A.; Doelsch, E.; Borschneck, D.; Olivi, L.; Dominici, C.; Grauby, O.; Woicik, J. C.; Bottero, J.-Y. Synthesis of Large Quantities of Single-Walled Aluminogermanate Nanotube. *J. Am. Chem. Soc.* **2008**, *130*, 5862–5863.
(28) Yucelen, G. I.; Choudhury, R. P.; Vyalikh, A.; Scheler, U.; Beckham, H. W.; Nair, S. Formation of Single-Walled Aluminosilicate Nanotubes from Molecular Precursors and Curved Nanoscale Intermediates. *J. Am. Chem. Soc.* **2011**, *133*, 5397–5412.
(29) Thill, A.; Maillet, P.; Guiose, B.; Spalla, O.; Belloni, L.; Chaurand, P.; Auffan, M.; Olivi, L.; Rose, J. Physico-Chemical Control over the Single- or Double-Wall Structure of Aluminogermanate Imogolite-like Nanotubes. *J. Am. Chem. Soc.* **2012**, *134*, 3780–3786.
(30) Paineau, E.; Krapf, M.-E. M.; Amara, M.-S.; Matskova, N. V.; Dozov, I.; Rouziere, S.; Thill, A.; Launois, P.; Davidson, P. A Liquid-Crystalline Hexagonal Columnar Phase in Highly-Dilute Suspensions of Imogolite Nanotubes. *Nat. Commun.* **2016**, *7*, 10271.
(31) Paineau, E.; Rouzière, S.; Monet, G.; Diogo, C. C.; Morfin, I.; Launois, P. Role of Initial Precursors on the Liquid-Crystalline Phase Behavior of Synthetic Aluminogermanate Imogolite Nanotubes. *J. Colloid Interface Sci.* **2020**, *580*, 275–285.
(32) Paineau, E.; Launois, P. Nanomaterials From Imogolite: Structure, Properties, and Functional Materials. In *Nanomaterials from Clay Minerals*; Elsevier, 2019; pp 257–284.
(33) Denaix, L.; Lamy, I.; Bottero, J. Y. Structure and Affinity towards Cd2+, Cu2+, Pb2+ of Synthetic Colloidal Amorphous Aluminosilicates and Their Precursors. *Colloids Surf. - Physicochem. Eng. Asp.* **1999**, *158*, 315–325.
(34) Yamada, H.; Michalik, J.; Sadlo, J.; Perlinska, J.; Takenouchi, S.; Shimomura, S.; Uchida, Y. Electron Spin Resonance Studies on Silver Atoms in Imogolite Fibers. *Appl. Clay Sci.* **2001**, *19*, 173–178.

(35) Kuroda, Y.; Fukumoto, K.; Kuroda, K. Uniform and High Dispersion of Gold Nanoparticles on Imogolite Nanotubes and Assembly into Morphologically Controlled Materials. *Appl. Clay Sci.* **2012**, *55*, 10–17.
(36) Liz-Marzán, L.; Philipse, A. P. Synthesis of Platinum Nanoparticles in Aqueous Host Dispersions of Inorganic (Imogolite) Rods. *Colloids Surf. Physicochem. Eng. Asp.* **1994**, *90*, 95–109.
(37) Liz-Marzán, L.; Philipse, A. Stable Hydrosols of Metallic and Bimetallic Nanoparticles Immobilized on Imogolite Fibers. *J. Phys. Chem.* **1995**, *99*, 15120–15128.
(38) Yucelen, G. I.; Connell, R. E.; Terbush, J. R.; Westenberg, D. J.; Dogan, F. Synthesis and Immobilization of Silver Nanoparticles on Aluminosilicate Nanotubes and Their Antibacterial Properties. *Appl. Nanosci.* **2016**, *6*, 607–614.
(39) Hsu, W.-J.; Ibrahim, I. A.; Lin, Y.-H.; Yang, Z.-H.; Yucelen, G. I.; Han, J. W.; Kang, D.-Y. Transparent Conductive Films Derived from Single-Walled Aluminosilicate Nanotubes. *ACS Appl. Nano Mater.* **2019**, *2*, 6677–6689.
(40) Amara, M.-S.; Paineau, E.; Bacia-Verloop, M.; Krapf, M.-E. M.; Davidson, P.; Belloni, L.; Levard, C.; Rose, J.; Launois, P.; Thill, A. Single-Step Formation of Micron Long (OH)3Al2O3Ge(OH) Imogolite-like Nanotubes. *Chem. Commun.* **2013**, *49*, 11284–11286.
(41) Paineau, E.; Amara, M. S.; Monet, G.; Peyre, V.; Rouzière, S.; Launois, P. Effect of Ionic Strength on the Bundling of Metal Oxide Imogolite Nanotubes. *J. Phys. Chem. C* **2017**, *121*, 21740–21749.
(42) Dubois, M.; Zemb, T.; Belloni, L.; Delville, A.; Levitz, P.; Setton, R. Osmotic Pressure and Salt Exclusion in Electrostatically Swollen Lamellar Phases. *J. Chem. Phys.* **1992**, *96*, 2278–2286.
(43) Tao, J.; Huang, N.; Li, J.; Chen, M.; Wei, C.; Li, L.; Wu, Z. Modulating the Arrangement of Charged Nanotubes by Ionic Strength in Salty Water. *J. Phys. Chem. Lett.* **2014**, *5*, 1187–1191.
(44) Ma, W.; Yah, W. O.; Otsuka, H.; Takahara, A. Application of Imogolite Clay Nanotubes in Organic-Inorganic Nanohybrid Materials. *J. Mater. Chem.* **2012**, *22*, 11887–11892.
(45) Li, L.; Ma, W.; Takada, A.; Takayama, N.; Takahara, A. Organic–Inorganic Hybrid Films Fabricated from Cellulose Fibers and Imogolite Nanotubes. *Biomacromolecules* **2019**, *20*, 3566–3574.
(46) Lee, W. J.; Paineau, E.; Anthony, D. B.; Gao, Y.; Leese, H. S.; Rouzière, S.; Launois, P.; Shaffer, M. S. P. Inorganic Nanotube Mesophases Enable Strong Self-Healing Fibers. *ACS Nano* **2020**, *14*, 5570–5580.
(47) Assender, H. E.; Windle, A. H. Crystallinity in Poly (Vinyl Alcohol). 1. An X-Ray Diffraction Study of Atactic PVOH. *Polymer* **1998**, *39*, 4295–4302.